

Dynamic mechanisms controlling the topography of Longmenshan area

Yuan XIE, Yongdong LI & Xiong XIONG*

*Hubei Subsurface Multi-Scale Imaging Key Laboratory, Institute of Geophysics and Geomatics,
China University of Geosciences, Wuhan 430074, China*

Received January 10, 2019; revised May 3, 2019; accepted June 13, 2019; published online August 9, 2019

Abstract The Longmenshan fault, which defines the eastern edge of the Tibetan Plateau, is one of the steepest margins of the plateau with a sharp elevation drop of about 4 km over a distance less than 100 km across the Longmenshan fault. The mechanism which is responsible for controlling and maintaining the elevation difference is highly debated. Using multiple observations including seismic velocity model, Moho depth, effective elastic thickness of the lithosphere, we conducted a quantitative study for elucidating the contributions from crust and lithospheric mantle by an integrated analysis of lithospheric isostasy and flexure. It is shown that the topography of the Longmenshan fault is supported by both lithospheric isostasy and flexure statically, and lower crustal channel flow and mantle convection dynamically. Different mechanisms have different weights for contribution to the topography of the Songpan-Ganzi block and the Sichuan Basin. The static and dynamic support contribute roughly the same to the topographic difference of ~4 km between the two sides of the Longmenshan fault. The static topographic difference of ~2 km is mainly resulted from the lithospheric isostasy, while the dynamic one of ~2 km is contributed by the uprising of the accumulated material in the lower crust beneath the Songpan-Ganzi block and the downward drag force caused by the upper mantle convection under the Sichuan Basin. It is thus suggested that the lower crustal flow and upper mantle convection are dynamic forces which should be taken into account in the studies on the dynamics in the Longmenshan and surrounding regions.

Keywords Topography, Longmenshan fault zone, Lithospheric isostasy, Lithospheric flexure, Dynamic topography

Citation: Xie Y, Li Y, Xiong X. 2020. Dynamic mechanisms controlling the topography of Longmenshan area. *Science China Earth Sciences*, 63: 121–131, <https://doi.org/10.1007/s11430-019-9380-2>

1. Introduction

Topography is among human's earliest and most intuitive observations about the Earth, and has richly informed us of the Earth's interior (e.g. the density, chemical composition, phases etc. of the crust, lithosphere and mantle) and dynamics (e.g. isostasy, mantle dynamics etc.) (Watts, 2001). Interpreting topographic signals helps us understand various issues in geodynamics, such as the structure of the crust and lithosphere (Jin et al., 1994; Wei et al., 2015), strength (Burov and Diament, 1995; Clark et al., 2005), crust-mantle

coupling (Clark et al., 2005; Bendick et al., 2008), and the mantle dynamics (Forte et al., 1993). Therefore, with strong curiosity and long passion men have been trying to probe into the mechanisms that sustain and control the topography.

In contrast to the oceanic topography, which can be roughly formulated by a cooling model in a semi-infinite half-space, the continental topography is much more complicated. The continent is as old as the Earth itself, and has experienced the whole tectonic evolution, resulting in a rather complex topography. Regions of such complexity are usually more tectonically active, and draw more attention for the abundant information they can provide, especially those with sharp elevation contrast, such as the Himalayan orogen

* Corresponding author (email: xxiong@cug.edu.cn)

and the Andean orogen.

The Longmenshan fault in China and its surroundings (Figure 1) as one of the most complicated and active regions in the world, have thus long been a focus of study. The Longmenshan region, which defines the eastern margin of the Tibetan plateau, with the Songpan-Ganzi fold belt to its northwest and the Sichuan Basin of the Yangtze craton to its southeast, is where the plateau and the neighboring blocks converge and interact. The Longmenshan fault sees an elevation drop of ~4000 m over a distance of less than 100 km, which means a sharp transition from plateau to plain. So what's the mechanism that sustains such a dramatic topography contrast?

Isostasy studies suggest that the Longmenshan area is not in Airy isostatic equilibrium (Braitenberg et al., 2000; Zhang et al., 2014), implying the involvement of other geodynamic processes. Studies on lithospheric flexural isostasy show that the gravity anomalies in Longmenshan region could be better explained by introducing the lithospheric flexural model with lateral variations of strength (Jiang and Jin, 2005), indicating that the topography of the Longmenshan area is at least partly supported by the isostasy and strength of the lithosphere. In addition to static support, some deep dynamic actions were suggested to be responsible for the elevation, such as channel flow in the lower crust and convection

within the upper mantle. Since no obvious Quaternary crustal shortening is observed on the eastern margin of the Tibetan plateau (Hubbard and Shaw, 2009), some studies suggest that (Royden et al., 1997) the mass accumulation due to the ongoing convergence between the Indian and Eurasian plates may have been absorbed in certain forms of interior deformation. The existence of a weak lower crust is proposed, so that material is transported outward from the Plateau as channel flow in the lower crust, while no shortening is observed in the upper crust. This model of lower crustal flow is successful in explaining the sharp topography contrast in the Longmenshan region in numerical modelling (Clark and Royden, 2000; Clark et al., 2005). Meanwhile, seismic tomography at depth exhibits small-scale convections underneath the eastern Plateau and the Sichuan Basin (Hirn et al., 1995; Li et al., 2008), and mantle material is found to be flowing eastward from the Plateau and aggregating below the Sichuan Basin (Xiong and Teng, 2002). Studies show that at least in some regions, mantle convection is dynamically supporting the topography (Liu et al., 2008; Becker et al., 2014).

These efforts have improved our understanding of the geodynamic mechanisms behind the topography in the Longmenshan region, yet there are many flaws. Firstly, the resolutions of the velocity and density models of this region

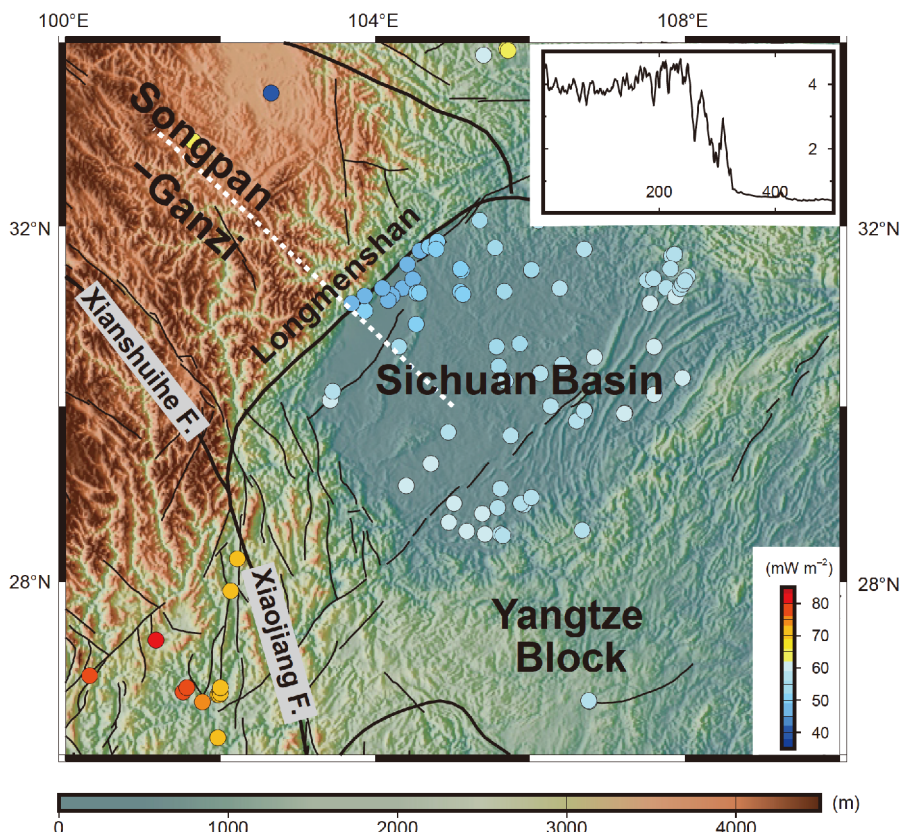


Figure 1 Topography of the Longmenshan fault and surrounding regions. The white dashed line is the profile of a receiver function study (Zhang et al., 2010). The circles indicate the locations of surface heat flow measurement, with the values colored by the scale. Inset shows the topography along the profile.

are limited, resulting in large uncertainties in isostasy and flexure analysis, thus different studies usually arrive at different conclusions. Moreover, while there are various studies based upon different mechanisms or models, integrated studies that include multiple mechanisms are rare. Due to the uncertainties of the interior structure and model parameters, a single model can often fit the observed topography by proper adjustments, impeding a comprehensive understanding through an integrated model. On the other hand, a series of geophysical observations nearby the eastern margin of the Tibetan Plateau provides us with increasingly abundant data, and new tomography technologies enable us to construct new velocity models of the interior structure with higher resolutions. With the progresses in observations and the ongoing theoretical studies about various mechanisms that control and support the topography, we are able to conduct a more advanced study than before.

In this paper, we combine the lithospheric structure (including the crustal thickness and the velocity model), lithospheric strength, topography, gravity and surface heat flow data into an integrated model that incorporates both static and dynamic support of the topography. Based on this model, we conduct lithospheric isostasy and flexure analysis to separate the contributions from the crust and mantle, then we discuss the dynamic mechanisms like lower crustal flow and deep mantle convection that support and control the topography of the Longmenshan region, attempting to achieve a more comprehensive understanding of this issue.

2. Model and method

The earliest studies on the dynamic mechanism responsible for topography could be traced back to the classic isostasy hypothesis (Watts, 2001), according to which the crust was assumed to be floating on the denser underlying mantle, namely the topography is supported by buoyancy. As the understanding of the Earth's interior structure developed, it was found that what floats on the asthenosphere is the lithosphere rather than the crust. Isostasy was thus suggested to be on the scale of the whole lithosphere (McNutt, 1990). In the isostasy hypothesis, the crust and lithosphere are idealized as separated prisms without interaction with each other. In reality, however, the lithosphere with lateral interaction has strength and bends in response to internal and external loadings, and such flexure partially supports/impedes the topography (Burov and Diament, 1995, 1996).

We now separate the static topography (H_{static}) from the observed topography (H), including the topography supported by hydrostatic isostasy (H_{iso}) and by flexure (H_{flex}). Then we define the difference between the observed topography and static topography as the residual topography (H_{res}), or the non-static topography ($H_{\text{non-static}}$), because this

part of topography derives from dynamic mechanisms such as mantle convection and so on. Accordingly, the observed topography H can be expressed as

$$\begin{aligned} H &= H_{\text{static}} + H_{\text{non-static}} \\ &= H_{\text{iso}} + H_{\text{flex}} + H_{\text{dyn}}. \end{aligned} \quad (1)$$

2.1 Lithospheric isostasy

According to the isostasy hypothesis, the lithosphere floats on the asthenosphere of uniform density ρ_a , achieving an equilibrium at the base of the lithosphere, thus the topography is supported by the buoyancy exerted on the lithosphere. This is an application of Archimedes' principle of hydrostatic equilibrium, which assumes that the buoyancy depends only on the lithospheric density $\rho(z)$ and thickness l (Lachenbruch and Morgan, 1990), hence the topography is given by

$$H_{\text{iso}} = \int_{-H}^L \frac{\rho_a - \rho(z)}{\rho_a} dz - H_0, \quad (2)$$

where z is measured positive downward; H is the observed topography; H_0 is the average depth of the mid-ocean ridges (2.4 km) (Lachenbruch and Morgan, 1990), and L is the integral depth or compensation depth. Theoretically, once L exceeds the depth of the bottom of the lithosphere, $\rho(z)$ in eq. (2) is equal to the density of the asthenosphere ρ_a , and H_{iso} derived from eq. (2) will no longer increase with L . Therefore, for regions without accurate thickness of the lithosphere, we only need to adopt a compensation depth greater than the maximum depth to obtain a reliable isostasy topography that represents contribution from the lithosphere as a whole. Specifically for the Longmenshan region, an estimated increase of lithosphere thickness from 70 to 150 km at the transition from the eastern margin of the Tibetan Plateau to the Sichuan Basin is revealed by a receiver function study (Zhang et al., 2010), we thus adopt a uniform compensation depth of 185 km.

Dividing the lithosphere into the crust with density $\rho_c(z)$ and thickness l_c and the lithospheric mantle with density of $\rho_m(z)$ (Figure 2), we are able to calculate their contributions to topography separately as H_c and H_m

$$H_c = \int_{-H}^{l_c} \frac{\rho_a - \rho_c(z)}{\rho_a} dz, \quad (3)$$

$$H_m = \int_{l_c}^L \frac{\rho_a - \rho_m(z)}{\rho_a} dz. \quad (4)$$

2.2 Lithospheric flexure

In contrast to the separated lithospheric prisms suggested by the classic isostasy hypothesis, the lithosphere in reality is characterized by lateral variations of strength, leading to

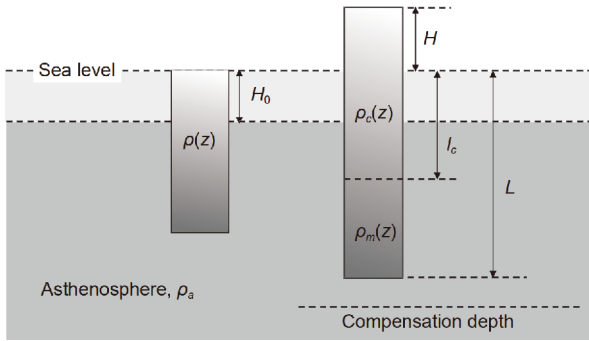


Figure 2 An illustration of the lithospheric isostasy hypothesis (Modified from Lachenbruch and Morgan (1990)). The symbols in the figure are explained in the text.

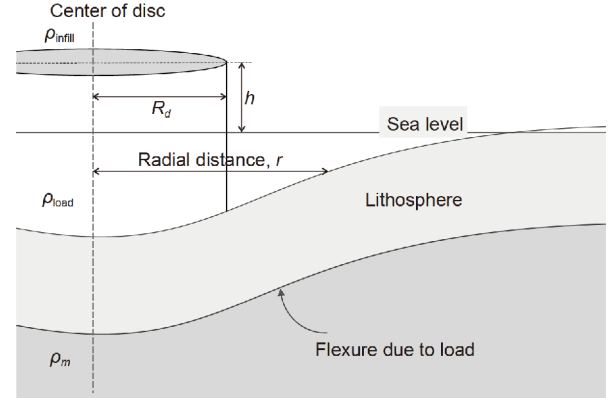


Figure 3 An illustration of the deflection of the lithosphere (Modified from Watts (2001)), and the symbols in the figure are explained in the text.

lateral interaction and flexure deformation (Barrell, 1914; Walcott, 1970). The strength of the continental lithosphere undermines the effect of isostasy, leading to uplifts lower than what classic isostasy models predict, and this is how the strength of the lithosphere contributes to the topography.

Elastic deformation of the lithosphere can be approximated as the bending of a thin elastic plate, whose response to a load $q(x)$ with a flexural rigidity $D(x)$ can be obtained by solving the general equation for the deflection of the plate (Turcotte and Schubert, 2002.)

$$\frac{\partial^2}{\partial x^2} \left[D(x) \frac{\partial^2 w}{\partial x^2} \right] + (\rho_m - \rho_c) g w = q(x), \quad (5)$$

where the load $q(x)$ depends on the density structure of the lithosphere; w is the deflection of the lithosphere in response to the load $q(x)$, and the flexural rigidity $D(x)$ is a measure of the lithosphere's stiffness or resistance to bending, which is generally characterized by the elastic thickness T_e as $D=ETe^3/12(1-\nu^2)$, and ν and E as Poisson's ratio and Young's modulus (Turcotte and Schubert, 2002) are given the values of 0.25 and 100 GPa respectively in this study. We adopt the Bessel function of zero order to approximate the damping effect of lithospheric strength (Watts, 2001):

$$\begin{cases} w = \frac{h\rho_{\text{load}}}{(\rho_m - \rho_{\text{infill}})} \left[\left(\frac{R_d}{\beta} \right) \text{ker}' \left(\frac{R_d}{\beta} \right) \text{ber} \left(\frac{r}{\beta} \right) \right. \\ \quad \left. - \left(\frac{R_d}{\beta} \right) \text{kei}' \left(\frac{R_d}{\beta} \right) \text{bei} \left(\frac{r}{\beta} \right) + 1 \right], & r < R_d, \\ w = \frac{h\rho_{\text{load}}}{(\rho_m - \rho_{\text{infill}})} \left[\left(\frac{R_d}{\beta} \right) \text{ber}' \left(\frac{R_d}{\beta} \right) \text{ker} \left(\frac{r}{\beta} \right) \right. \\ \quad \left. - \left(\frac{R_d}{\beta} \right) \text{bei}' \left(\frac{R_d}{\beta} \right) \text{kei} \left(\frac{r}{\beta} \right) \right], & r > R_d, \end{cases} \quad (6)$$

where ρ_{load} and ρ_{infill} (we assume $\rho_{\text{infill}}=0$) are respectively the density of the load and the overlying layer; ber , bei , ker and kei are Bessel-Kelvin functions; h , R_d and r are respectively the height, radius and the radial distance of the calculated point from the load; and β is the flexural parameter (Figure 3):

$$\beta = \left[\frac{D}{(\rho_m - \rho_{\text{infill}})g} \right]^{1/4}. \quad (7)$$

2.3 Data

Various data sets from multiple sources are used in this paper, includingETOPO1 global relief model (<https://www.ngdc.noaa.gov>), Moho depth models (Li et al., 2014; Zhang et al., 2010) (Figure 4a), the effective elastic thickness of the lithosphere (Li et al., 2013) (Figure 4b), surface heat flow (Jiang et al., 2016) and a seismic velocity model (Shen et al., 2016), which enjoys the highest resolution available for the study region ($0.5^\circ \times 0.5^\circ$) as it is jointly inverted by ambient noise Rayleigh wave tomography and receiver functions using data from dense arrays.

2.4 Estimate of density

In this section, we convert the seismic velocity model to a density model based on velocity-density empirical scaling relationships. Given the discrepancy between the composition of the crust and the lithospheric mantle, different empirical relationships are adopted.

We assume a compositionally homogeneous lithospheric mantle with a reference shear velocity V_{ref} of 4.3 km s^{-1} and a reference density ρ_{ref} of 3200 kg m^{-3} . Under an assumption that the variations of velocity and density are both thermal in origin, a velocity perturbation scales to a density perturbation as (Levandowski et al., 2015)

$$\begin{cases} \Delta\rho = \Delta V_S \times \left(7.3 - \frac{z}{100 \text{ km}} + \frac{\Delta V_S}{4} \right), \\ \Delta V_S \leq 6\%, \\ \Delta\rho = \Delta V_S \times \left(8.8 - \frac{z}{100 \text{ km}} + \frac{7 \times (\Delta V_S - 6)}{40} \right), \\ \Delta V_S \geq 6\%, \end{cases} \quad (8)$$

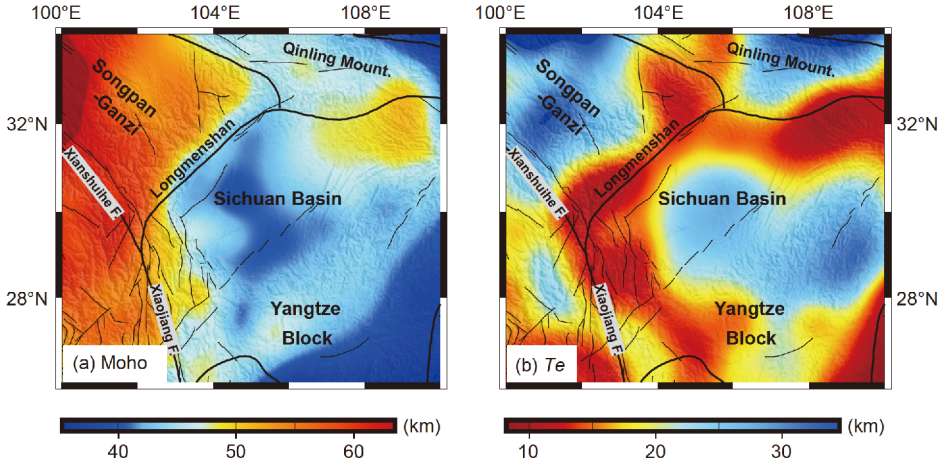


Figure 4 (a) The Moho depth (Li et al., 2014; Zhang et al., 2010) and (b) the effective elastic thickness of the lithosphere (Li et al., 2013).

where z is depth, and ΔV_S and $\Delta\rho$ are respectively velocity and density deviations from the reference values.

As for the crust, density can be obtained by the following empirical relationship with shear velocity V_S (Levandowski et al., 2015)

$$\rho = 2153.06 - 1163.00V_S + 1863.36V_S^2 - 961.94V_S^3 + 209.13V_S^4 - 15.84V_S^5 \quad (9)$$

Eq. (9) is an empirical velocity-density scaling relationship estimated from a regression of experimental data in rock physics, which is suited to intermediate compositions between the felsic and mafic rocks and reflects the global average velocity-density relationship in the crust. For a specific study region, relationship may deviate from what is described by eq. (9), thus assessments and corrections are necessary for a density model obtained by eq. (9) to minimize such deviation.

Given that gravity is the most sensitive quantity to the density of compositions of the Earth, a density model as a

good approximation of the reality should produce gravity anomalies consistent with observed. Compared to the crust, the lithospheric mantle is of relatively homogeneous composition, and density perturbations mainly arise from temperature perturbations, and the lithospheric mantle makes relatively small contribution to gravity anomalies. However, for cratonic lithospheric mantle, the compositional structure has a great impact on density, thus we refer to a compositional study about the lithospheric mantle of Sichuan Basin, which showed that it has $Mg^{\#}$ of 89–90 (Shan et al., 2014), a value falling into the composition range of normal lithospheric mantle and does not exhibit significant loss or enrichment of magnesium. We thus conclude that the effect of the composition of the mantle on density in Sichuan Basin is small. Accordingly, we correct the density model of the crust by fitting it to the observed Bouguer gravity anomaly with residuals under ± 8 mGal (Figure 5a), so as to obtain corrections for the average density of the crust (Figure 5b). The density model after such correction was applied to the cal-

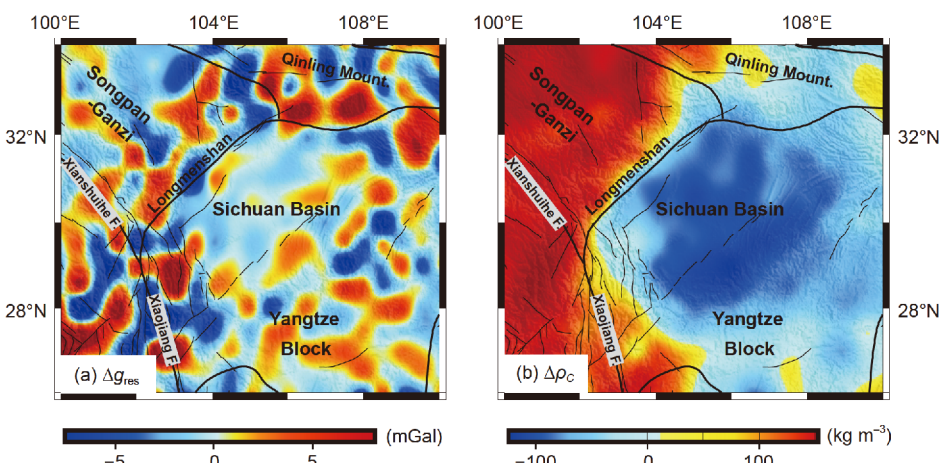


Figure 5 (a) Residuals of the Bouguer gravity anomaly and (b) corrections for the average density of the crust.

culation of lithosphere isostasy and flexure.

3. Results

3.1 Contribution of lithospheric isostasy

The contribution of the lithosphere as a whole and the respective contribution of the crust and lithospheric mantle to the topography are calculated using the density model with corrections and eq. (2) (Figure 6). We found that the contribution of the crust is between 4.5 to 7.6 km, and the value specifically can be more than 7 km in the Songpan-Ganzi block, while for the Sichuan Basin it is between 5.5 and 6.5 km (Figure 6a). Thus, there is approximately 1 km difference between the two sides of the Longmenshan fault regarding the crust's contribution to the topography.

The contribution of the lithospheric mantle is mostly negative, indicating a $-2.8\text{--}0.2$ km topography dragged downward by negative buoyancy in the mantle. The magnitude of this topography component is larger in the Sichuan basin ($-2.8\text{--}2.0$ km) and less in the Songpan-Ganzi block ($-2\text{--}0.2$ km), resulting in a topography difference of -2 km caused by the lithospheric mantle between the two sides of the Longmenshan fault (Figure 6b).

The sum of the contributions of the crust and the lithospheric mantle minus the average depth of the mid-ocean ridge (2.4 km) (Lachenbruch and Morgan, 1990) gives the contribution of lithospheric isostasy to topography (H_{iso}) (Figure 6c), which is overall positive in the study region, revealing an upward support to the topography from density perturbations of the lithosphere. Such contribution of lithospheric isostasy varies in space, with a gradual decrease from above 2.0 km in the northwestern Songpan-Ganzi block to 0.5–2.0 km in the southeastern Sichuan Basin.

3.2 Contributions of lithospheric flexure and static topography

Given the strength of the lithosphere (Li et al., 2013) and loads as a result of the density structure, the damping effect induced by such strength can be obtained through eq. (6), and the flexure contributes to topography in this way. In the study region, such contribution ranges from -1.6 to 0 km, with higher values in the west due to the large vertical loads caused by the density structure of the lithosphere on the eastern margin of the Tibetan Plateau. As regards the Sichuan Basin, due to the high lithospheric strength and low load, the contribution of the strength of the lithosphere is generally below 0.5 km (Figure 7). As a result, there is a topography difference >0.8 km between the two sides of the Longmenshan fault.

Adding the topography supported by lithospheric flexure (Figure 7) to isostasy topography (Figure 6c) gives what we

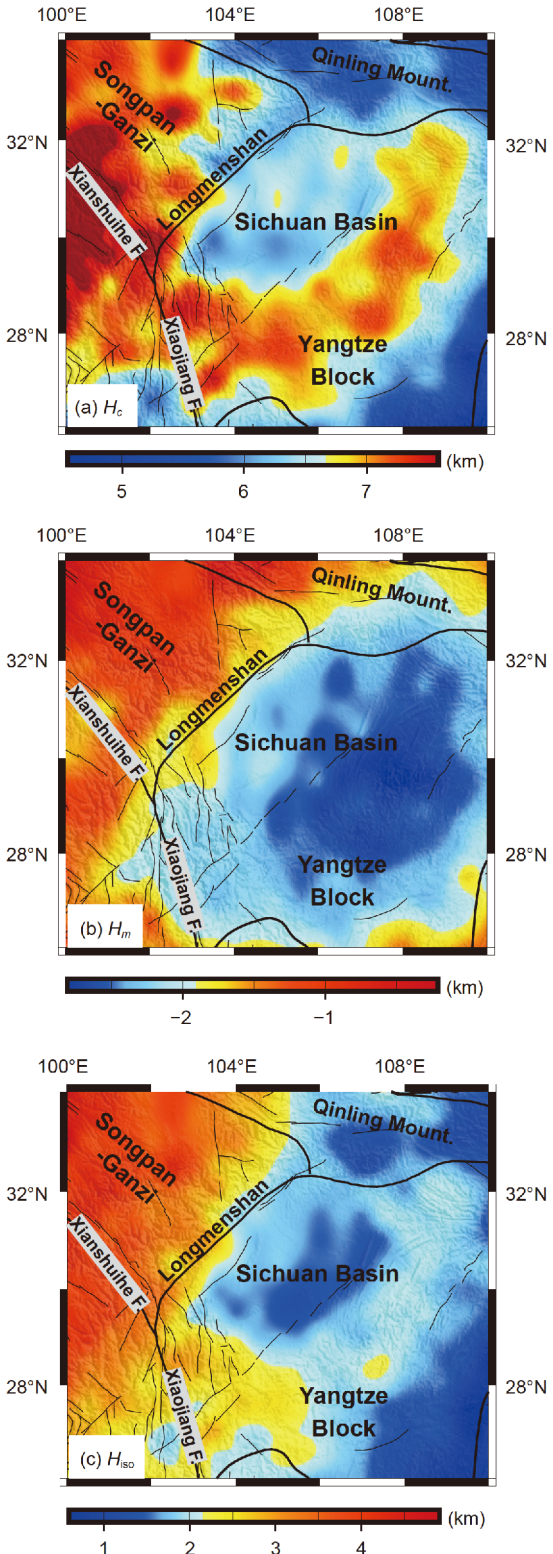


Figure 6 Isostasy contributions to the topography of (a) the crust, (b) the lithospheric mantle and (c) the lithosphere as a whole.

define as static topography (Figure 8), which ranges from 0.5 to 3.7 km. Specifically in the study region, from the Songpan-Ganzi fold belt in the eastern margin of the Tibet plateau

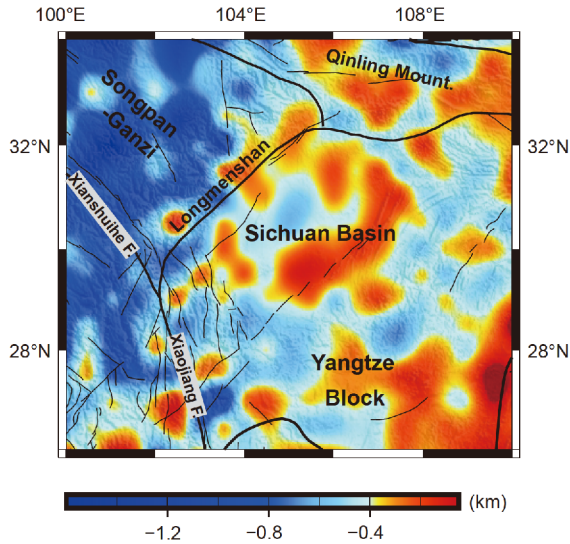


Figure 7 Topography supported by lithospheric flexure.

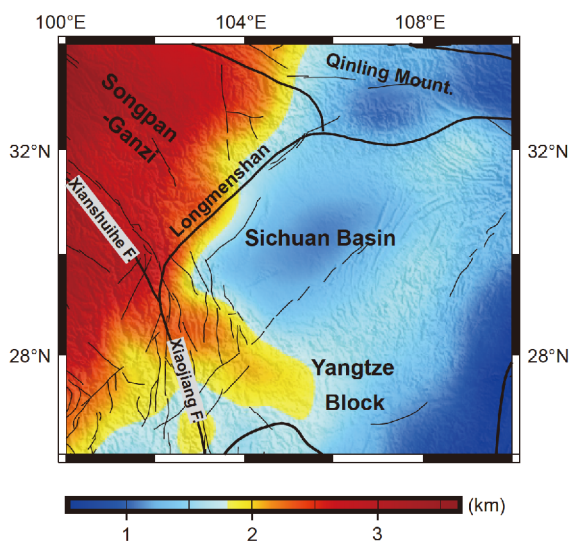


Figure 8 The static topography of the Longmenshan region.

to the Sichuan Basin and the Yangtze Craton, the static topography decreases from about 3.0 km to a minimum of 0.5 km, resulting in a 2 km difference in static topography between the two sides of the Longmenshan fault.

3.3 Dynamic topography

Removing static topography from the observed topography gives the non-static topography ($H_{\text{non-static}}$), or dynamic topography (H_{dyn}) (Flament et al., 2013; Becker et al., 2014; Molnar et al., 2015). As illustrated in Figure 9, there is about 2 km of difference in dynamic topography between the two sides of the Longmenshan fault, with Sichuan Basin of negative values <-0.5 km, and Songpan-Ganzi block of positive

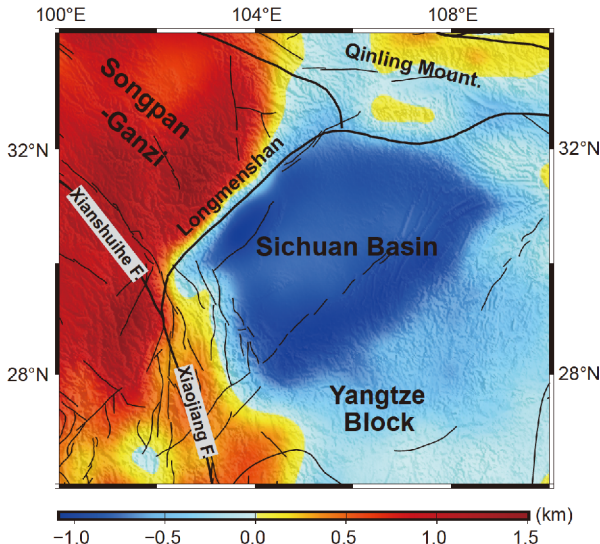


Figure 9 Dynamic topography in the Longmenshan region.

tive values of 0–1.5 km.

4. Discussion

4.1 Thermal and compositional contributions of crust to topography

The physical properties of the Earth (including seismic velocity and density) are influenced by several factors, such as temperature, pressure, phases, composition and so on. Given that the lithospheric mantle can be regarded incompressibility for which influence from pressure is negligible, and that its phases and composition are relatively homogeneous, its physical properties depends primarily on temperature. For the crust, the influence of pressure is also negligible (Christensen, 1996), and the phases change (partial melting) only has localized impacts, thus what controls the physical properties of the crust are temperature and chemical composition of the rocks. Since topography is the surface expression of the physical properties of the Earth's interior, separating different factors that contribute to topography helps us elucidate the weights of various factors in determining the physical properties of the Earth.

We calculated the thermal and compositional contributions of the crust to topography respectively. Assuming a surface temperature of 20°C, we can derive the temperature perturbation ΔT in the crust from the value of surface heat flow, whose topographic contribution (H_{c-T}) can be calculated by (Levandowski et al., 2014)

$$H_{c-T} = \int_0^{l_c} \frac{\rho_c(z) \alpha \Delta T}{\rho_a} dz, \quad (10)$$

where α is the coefficient of thermal expansion (usually assumed to be $2.5 \times 10^{-5} \text{ }^{\circ}\text{C}^{-1}$). Next, we have

$$H_{c-C} = H_c - H_{c-T}, \quad (11)$$

to obtain the compositional contribution of the crust (H_{c-C}).

Since the measuring points of heat flow are not evenly distributed over the study region, there are certain areas where no measuring points are available to construct constraints for a complete 3-D temperature model. Thus, we only calculated H_{c-C} at the measuring points, and the result ranges from -0.2 – 0.27 km (Figure 10a) and shows a positive correlation with the surface heat flow. As shown in Figure 1, the measuring points are concentrated in the Sichuan Basin, with measured values ranging from 50 to 60 mW m $^{-2}$ and the corresponding H_{c-T} -0.2 – 0 km. In contrast, the Songpan-Ganzi block has only two points with measured values of 41 and 64 mW m $^{-2}$, the corresponding H_{c-T} of which are -0.2 km and 0 km. In addition, the heat flow values measured west of the Xiaojiang fault are as high as 65 – 80 mW m $^{-2}$, corresponding to H_{c-T} above 0.1 km.

Removing H_{c-T} from H_c gives the compositional contribution of the crust to the topography, namely the H_{c-C} (Figure 10b), whose value is between 4.5 to 7.1 km in the study region, and specifically 5 – 7 km in the Sichuan Basin. We can see that the contribution of composition variations is higher than that of temperature perturbations by almost an order of magnitude, thus the crustal contribution to topography is obviously compositional. This observation also reveals the decisive role of composition in the density structure of the crust.

4.2 Robustness of results

The observational datum and numerical models (the density model and effective elastic thickness of the lithosphere, the Moho depth model and surface heat flow) all introduce uncertainties to the calculations, making it necessary to conduct tests to assess their effects on the results.

The density model of lithosphere was constructed based on

the empirical velocity-density scaling relations and was corrected by comparing it to the observed gravity anomalies. Thus, the errors caused by uncertainties of the density model are reflected in the residual gravity anomalies, which fall within ± 8 mGal as is calculated in Section 2.4. Assuming a crust thickness of 40 km, we obtain a density anomaly of 4.77 kg m $^{-3}$ corresponding to an 8 mGal gravity anomaly. Given that a 4.77 kg m $^{-3}$ density anomaly contributes to topography by about 0.06 km, we conclude that the errors induced by uncertainties in the density model are less than 0.06 km.

Generally the uncertainty in crustal thickness (namely the Moho depth) derived from receiver functions is about ± 4 km, and the kriging interpolation based upon receiver function data produces an uncertainty of ± 2 km (Li et al., 2014). Assuming a linear propagation of errors, the combination of the two uncertainties gives a total of ± 6 km (Li et al., 2014). We calculated topography caused by the ± 6 km error in the Moho depth, and the result is shown in Figure 11a, which ranges from -0.05 to 0.60 km with an average uncertainty of 0.27 km. 95.8% of the values are within the extent of 0 – 0.5 km, and 83.1% within 0 – 0.40 km.

Errors may also arise from uncertainties in lithospheric strength. Given that the elastic thickness (T_e) of the lithosphere over the entire region ranges from 10 to 35 km with a maximum error less than 4 km (Li et al., 2013), we assume a $\pm 10\%$ variation of T_e and calculated the uncertainty of topography supported by lithospheric flexure H_{flex} , and the result is within the extent of -0.02 – 0.02 km with an average uncertainty of 0 km. Since 98.9% of the values are within ± 0.01 km, such uncertainty is negligible.

The uncertainty of surface heat flow has no impact on static and residual topography. Moreover, the thermal contribution from the crust based on heat flow is about -0.20 – 0.27 km, which is an order of magnitude smaller than the compositional contribution. In other words, even a 100%

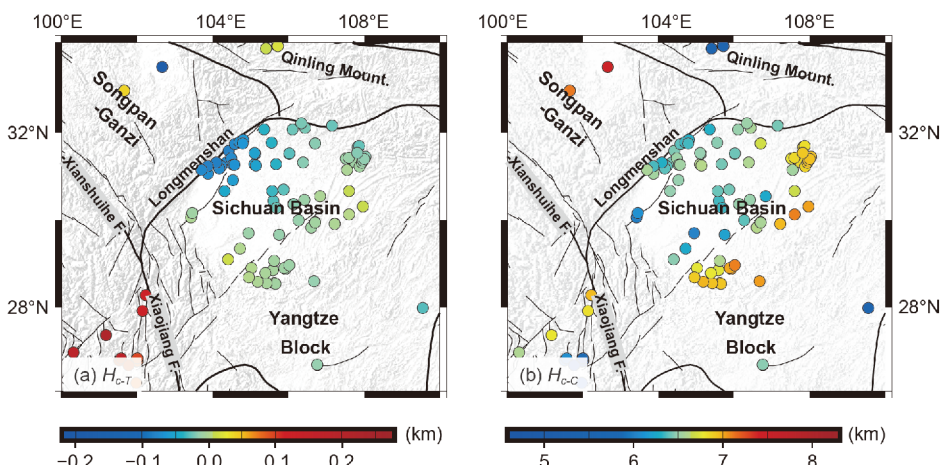


Figure 10 Topographic contributions of crustal (a) temperature perturbations and (b) composition inhomogeneous.

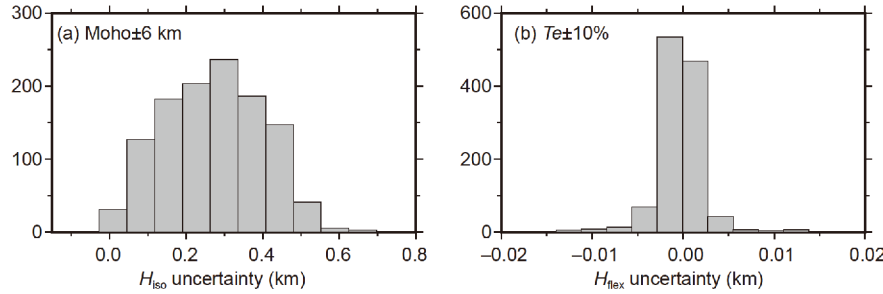


Figure 11 Statistical analysis of uncertainties.

uncertainty in heat flow cannot undermine the dominant role of compositional contribution to topography.

Given that the static topography is a linear superposition of contributions from various mechanisms, the above statistical discussions about errors are also subject to the superposition principle, the combination of which gives a maximum average error of 0.33 km.

4.3 Mechanisms supporting dynamic topography

In order to understand the forces and mechanisms that support the dynamic topography in the Longmenshan region in a more intuitive way, we calculated static and dynamic topography along a profile crossing the Longmenshan fault (Figure 1) based on the information it provides about the Moho depth and LAB. As is illustrated in Figure 12, the topographic difference between the Songpan-Ganzi block and the Sichuan Basin is significant: the H_{dyn} of the Songpan-Ganzi (colored pink) is 1–1.5 km, while that of the Sichuan Basin (colored blue) is −0.5 km, resulting in a difference of 2 km.

Studies agree that the major deep dynamics at depth in the Longmenshan region are the lower crustal flow beneath the eastern margin of the Tibetan Plateau (Royden et al., 1997; Beaumont et al., 2001; Wang et al., 2008; Zhang, 2008), and small-scale mantle convections under the Tibetan Plateau and surrounding regions (Hirn et al., 1995; Li et al., 2008; Xiong and Teng, 2002).

The lower crustal flow model (Beaumont et al., 2001; Clark and Royden, 2000) assumes that the lower crust under the eastern margin of the Tibetan Plateau, with a low viscosity of $\sim 10^{18}$ Pa·s, is driven to the east by the pressure of the weight of the Tibetan Plateau, and is then obstructed as it encounters the rigid Sichuan Basin (with a viscosity of $\sim 10^{21}$ Pa·s). As a result, the mass flowing eastward accumulates along the Longmenshan fault and forms an abrupt uplift. Numerical modelling (Clark et al., 2005) reveals a possible topography anomaly as high as 1.5 km as a result of lower crustal flow, which is consistent with the 1–1.5 km dynamic topography we obtained on the eastern margin of the Tibetan Plateau.

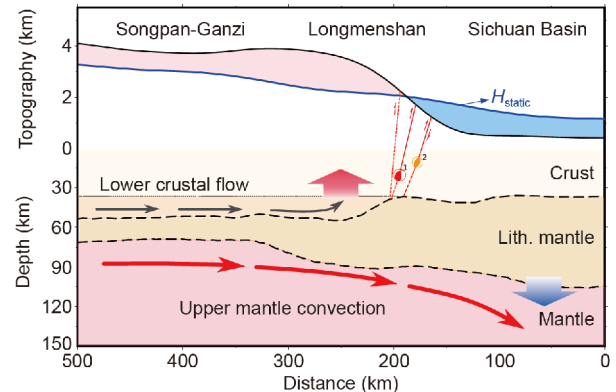


Figure 12 An illustration of the observed and static topography, as well as deep dynamics along a profile of the Longmenshan fault system. The solid black and blue lines indicate respectively the observed topography and static topography, and the areas colored pink and blue indicate respectively positive and negative dynamic topography; the dashed black lines denote the Moho and LAB; the grey arrows indicate the directions to which the lower crustal material moves, and the red arrows indicate the convective flow of the upper mantle; the No. 1 and No. 2 focal mechanisms correspond respectively to the 2008 M_w 7.9 Wenchuan earthquake and the 2013 M_w 6.6 Lushan earthquake; the thin red lines are cross-sections of some faults in the Longmenshan fault system, with the dashed lines indicating speculative faults.

Seismic tomography models (Hirn et al., 1995; Li et al., 2008) and gravity inversion (Xiong and Teng, 2002) suggest the existence of an active convection system within the upper mantle under the Tibetan Plateau and surrounding regions. The mantle flow upwells under the Northern Tibet and then disperses to all directions, out of the plateau from the eastern margin, through the Longmenshan fault system and descends in the Sichuan Basin. Such convection of the mantle produces stress at the base of the lithosphere, resulting in the deformation thereof, which in turn causes topography changes (Liu, 1978). Supposing the dynamic topography of the Sichuan Basin is attributed to the convection-generated stress at the base of the lithosphere, we estimate the magnitude of such stress to be 20–45 MPa (Figure 13) by solving eq. (5) the general equation for the deflection of the plate. Mantle convections also induce corresponding stress field at the base of the lithosphere beneath the eastern margin of the Tibetan Plateau, but the low viscosity of the lower crust

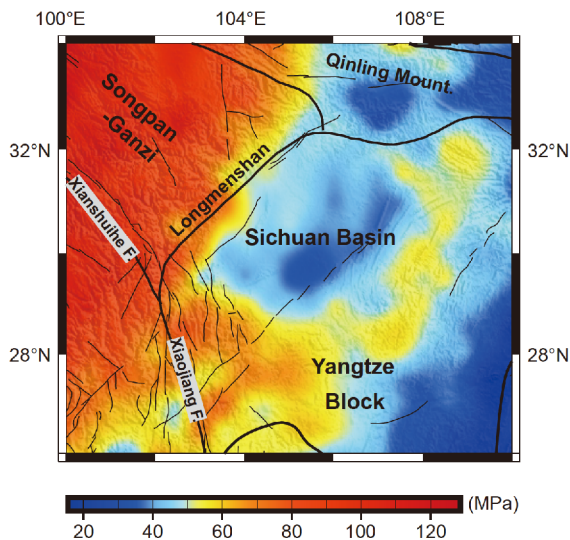


Figure 13 Magnitude of stress at the base of the lithosphere converted from dynamic topography.

thereof undermines crust-mantle coupling or even leads to decoupling, so that the stress induced by mantle convection cannot be transferred to the upper crust. As a result, mantle convection makes little topographic contribution on the eastern margin of the Tibetan Plateau, whose dynamic topography is mostly attributed to lower crustal flow.

In summary, lower crustal flow west of the Longmenshan fault system produces ~ 1.5 km uplift, while descending mantle flow on the eastern side as part of the mantle convection system creates about -1 km dynamic topography, resulting in a topographic difference of about 2 km.

5. Conclusion

In this study, we analyzed different mechanisms that are responsible for the topography of Longmenshan region. Combining calculations based upon both lithospheric isostasy and flexure with investigations of dynamic processes in this region including lower crustal flow and mantle convection, we come up with the following conclusions:

(1) Major mechanisms that control the topography of the Longmenshan region include static support from lithospheric isostasy and flexure, and dynamic support including lower crustal flow and mantle convection. These mechanisms weigh differently in different blocks: in the Songpan-Ganzi block, lithospheric isostasy and lithospheric flexure respectively contributes >7 km and about -1.2 km static topography, and lower crustal flow contributes $1\text{--}1.5$ km dynamic topography; while in the Sichuan Basin, the contributions from lithospheric isostasy and lithospheric flexure are respectively $0.5\text{--}2$ km and around -0.4 km, and it is mantle convection that causes dynamic topography of a magnitude of approximately -1 km.

(2) Static and dynamic topography make roughly equivalent contributions to the ~ 4 km topography difference between the two sides of the Longmenshan fault, with the ~ 2 km static contribution coming primarily from lithospheric isostasy and the ~ 2 km dynamic contribution as an integration of the uplift caused by the mass accumulation due to lower crustal flow underneath the Songpan-Ganzi block and the depression caused by the downward dragging force due to the mantle convection underneath the Sichuan Basin.

(3) The compositional contribution of the crust to topography is an order of magnitude greater than thermal contribution, implying a major role of the compositions of crustal rocks in determining the density structure of the crust.

(4) The existence of dynamic topography indicates the necessity to take lower crustal flow and mantle convection into consideration in geodynamic studies on the Longmenshan fault and adjacent regions.

Acknowledgements We thank Dr. Weisen Shen of University of Colorado at Boulder for the seismic tomography data set, and anonymous reviewers for their insightful review and thoughtful comments. We thank Ms. Yashan Feng for editing the English version of the manuscript. Most figures were prepared with the Generic Mapping Tools (Wessel and Smith, 1998). This work was supported by the National Key R & D Program of China (Grant No. 2017YFC1500305) and the National Natural Science Foundation of China (Grant Nos. 41731072 & 41574095).

References

- Barrell J. 1914. The strength of the Earth's crust. *J Geol*, 22: 655–683
- Beaumont C, Jamieson R A, Nguyen M H, Lee B. 2001. Himalayan tectonics explained by extrusion of a low-viscosity crustal channel coupled to focused surface denudation. *Nature*, 414: 738–742
- Becker T W, Faccenna C, Humphreys E D, Lowry A R, Miller M S. 2014. Static and dynamic support of western United States topography. *Earth Planet Sci Lett*, 402: 234–246
- Bendick R, McKenzie D, Etienne J. 2008. Topography associated with crustal flow in continental collisions, with application to Tibet. *Geophys J Int*, 175: 375–385
- Braitenberg C, Zadro M, Fang J, Wang Y, Hsu H T. 2000. The gravity and isostatic Moho undulations in Qinghai-Tibet Plateau. *J Geodyn*, 30: 489–505
- Burov E B, Diament M. 1995. The effective elastic thickness (T_e) of continental lithosphere: What does it really mean? *J Geophys Res*, 100: 3905–3927
- Burov E B, Diament M. 1996. Isostasy, equivalent elastic thickness, and inelastic rheology of continents and oceans. *Geology*, 24: 419–422
- Christensen N I. 1996. Poisson's ratio and crustal seismology. *J Geophys Res*, 101: 3139–3156
- Clark M K, Bush J W M, Royden L H. 2005. Dynamic topography produced by lower crustal flow against rheological strength heterogeneities bordering the Tibetan Plateau. *Geophys J Int*, 162: 575–590
- Clark M K, Royden L H. 2000. Topographic ooze: Building the eastern margin of Tibet by lower crustal flow. *Geology*, 28: 703–706
- Flament N, Gurnis M, Muller R D. 2013. A review of observations and models of dynamic topography. *Lithosphere*, 5: 189–210
- Forte A M, Peltier W R, Dziewonski A M, Woodward R L. 1993. Dynamic surface topography: A new interpretation based upon mantle flow models derived from seismic tomography. *Geophys Res Lett*, 20: 225–228
- Hirn A, Jiang M, Sapin M, Diaz J, Nercessian A, Lu Q T, Lépine J C, Shi D N, Sachpazi M, Pandey M R, Ma K, Gallart J. 1995. Seismic anisotropy

- as an indicator of mantle flow beneath the Himalayas and Tibet. *Nature*, 375: 571–574
- Hubbard J, Shaw J H. 2009. Uplift of the Longmen Shan and Tibetan plateau, and the 2008 Wenchuan ($M_w=7.9$) earthquake. *Nature*, 458: 194–197
- Jiang G Z, Gao P, Rao S, Zhang L Y, Tang X Y, Huang F, Zhao P, Pang Z H, He L J, Hu S B, Wang J Y. 2016. Compilation of heat flow data in the continental area of China (4th ed) (in Chinese). Chin J Geophys, 59: 2892–2910
- Jiang X D, Jin Y. 2005. Mapping the deep lithospheric structure beneath the eastern margin of the Tibetan Plateau from gravity anomalies. *J Geophys Res*, 110: B07407
- Jin Y, McNutt M K, Zhu Y S. 1994. Evidence from gravity and topography data for folding of Tibet. *Nature*, 371: 669–674
- Lachenbruch A H, Morgan P. 1990. Continental extension, magmatism and elevation; formal relations and rules of thumb. *Tectonophysics*, 174: 39–62
- Levandowski W, Boyd O S, Briggs R W, Gold R D. 2015. A random-walk algorithm for modeling lithospheric density and the role of body forces in the evolution of the Midcontinent Rift. *Geochem Geophys Geosyst*, 16: 4084–4107
- Levandowski W, Jones C H, Shen W S, Ritzwoller M H, Schulte-Pelkum V. 2014. Origins of topography in the western U.S.: Mapping crustal and upper mantle density variations using a uniform seismic velocity model. *J Geophys Res-Solid Earth*, 119: 2375–2396
- Li C, van der Hilst R D, Engdahl E R, Burdick S. 2008. A new global model for P wave speed variations in Earth's mantle. *Geochem Geophys Geosyst*, 9: Q05018
- Li Y D, Zheng Y, Xiong X, Hu X Y. 2013. Lithospheric effective elastic thickness and its anisotropy in the northeast Qinghai-Tibet Plateau (in Chinese). Chin J Geophys, 56: 1132–1145
- Li Y H, Gao M T, Wu Q J. 2014. Crustal thickness map of the Chinese mainland from teleseismic receiver functions. *Tectonophysics*, 611: 51–60
- Liu H S. 1978. Mantle convection pattern and subcrustal stress field under Asia. *Phys Earth Planet Inter*, 16: 247–256
- Liu L J, Spasojevic S, Gurnis M. 2008. Reconstructing Farallon plate subduction beneath North America back to the Late Cretaceous. *Science*, 322: 934–938
- McNutt M. 1990. Flexure reveals great depth. *Nature*, 343: 596–597
- Molnar P, England P C, Jones C H. 2015. Mantle dynamics, isostasy, and the support of high terrain. *J Geophys Res-Solid Earth*, 120: 1932–1957
- Royden L H, Burchfiel B C, King R W, Wang E, Chen Z L, Shen F, Liu Y P. 1997. Surface deformation and lower crustal flow in eastern Tibet. *Science*, 276: 788–790
- Shan B, Afonso J C, Yang Y, Grose C J, Zheng Y, Xiong X, Zhou L. 2014. The thermochemical structure of the lithosphere and upper mantle beneath south China: Results from multiobservable probabilistic inversion. *J Geophys Res-Solid Earth*, 119: 8417–8441
- Shen W S, Ritzwoller M H, Kang D, Kim Y, Lin F, Ning J Y, Wang W T, Zheng Y, Zhou L Q. 2016. A seismic reference model for the crust and uppermost mantle beneath China from surface wave dispersion. *Geophys J Int*, 206: 954–979
- Turcotte D L, Schubert G. 2002. *Geodynamics*. 3rd ed. Cambridge: Cambridge Univ Press. 133–162
- Walcott R I. 1970. Flexural rigidity, thickness, and viscosity of the lithosphere. *J Geophys Res*, 75: 3941–3954
- Wang C Y, Lou H, Lü Z Y, Wu J P, Chang L J, Dai S G, You H C, Tang F T, Zhu L P, Silver P. 2008. S-wave crustal and upper mantle's velocity structure in the eastern Tibetan Plateau—Deep environment of lower crustal flow. *Sci China Ser D-Earth Sci*, 51: 263–274
- Watts A B. 2001. *Isostasy and Flexure of the Lithosphere*. Cambridge: Cambridge University Press. 1–111
- Wei Z G, Chu R S, Chen L. 2015. Regional differences in crustal structure of the North China Craton from receiver functions. *Sci China Earth Sci*, 58: 2200–2210
- Wessel P, Smith W H F. 1998. New, improved version of generic mapping tools released. *Eos Trans AGU*, 79: 579
- Xiong X, Teng J W. 2002. Study on crustal movement and deep process in eastern Qinghai-Xizang Plateau (in Chinese). Chin J Geophys, 45: 507–515
- Zhang P Z. 2008. The present tectonic deformation in the Western Sichuan Area in the east margin of the Qinghai-Tibetan Plateau (in Chinese). *Sci China Ser D-Earth Sci*, 38: 1041–1056
- Zhang Y Q, Teng J W, Wang Q S, Hu G Z. 2014. Density structure and isostatic state of the crust in the Longmenshan and adjacent areas. *Tectonophysics*, 619–620: 51–57
- Zhang Z J, Yuan X H, Chen Y, Tian X B, Kind R, Li X Q, Teng J W. 2010. Seismic signature of the collision between the east Tibetan escape flow and the Sichuan Basin. *Earth Planet Sci Lett*, 292: 254–264

(Responsible editor: Dinghui YANG)